Electric Power Systems Research 257 (2026) 112954

Contents lists available at ScienceDirect

Electric Power Systems Research

journal homepage: www.elsevier.com/locate/epsr

NIDI: A robust system for identifying distortion and imbalance sources in microgrids

Reyes Sánchez-Herrera, Gabriel Gómez-Ruiz, Jesús Clavijo-Camacho *, José A. Hernández-Torres, Álvaro Cruz-Álamo, Nicolás Magro, Jesús R. Vázquez

Research Centre CITES of the University of Huelva, Huelva 21007, Spain

ARTICLE INFO

Keywords:
Distortion sources
Electrical measurements
Harmonic sources
Imbalance sources
Microgrids
Power quality disturbances
WebSocket

ABSTRACT

Electric power quality is becoming increasingly important over time due to the growing use of electronic devices across various sectors of society, including industry and households. Numerous disturbances can occur in the power grid due to both external and internal causes, such as switching devices on and off. Among these disturbances, distortion and imbalance are particularly problematic because they are pseudo-permanent disturbances, making them very dangerous for electrical equipment. Moreover, identifying the sources of distortion and/or imbalance is quite challenging because they are instantaneously scattered throughout the grid. This paper presents a complete experimental prototype designed to identify both distortion and imbalance sources in a microgrid, which would allow for their compensation at the node of origin. The proposed system comprises all necessary hardware and software, and is based on low-cost, free-software and open hardware. Simulation and experimental results are presented, each demonstrating the system's performance.

1. Introduction

According to a European power quality survey [1], power quality (PQ) issues cause a financial loss of more than EUR 150 billion per year in the 25 countries of the EU. These losses are due to devastating effects in loads and generation, transmission and distribution systems, such as damage of sensitive loads, loss of efficiency of the power system and overheating of cables and equipment, among others [2].

The power quality disturbances (PQDs) are classified into magnitude variations (voltage sags and swells), sudden transients (impulsive and oscillatory) and steady-state variations (harmonics, notch and flicker), and their definitions and compatibility levels are contained in the EN 50,160:2022 [3] for low, medium, high and extra-high voltage supply.

Among them, harmonic distortion is one of the most common PQDs and has become increasingly important in recent years due to the rising introduction of non-linear and time-varying loads in the power systems [4]. The proliferation of renewable energy systems (RES), facilitated by distributed generation (DG), exacerbates the issue of harmonics. For instance, power converters connecting these RESs to the power system not only generate harmonics but also introduce imbalances during operation. Note that any of RES are single-phase. One characteristic that makes the study of distortion and imbalance crucial is their inevitable propagation through different electrical microgrids and the power system. In addition, certain components present in these installations may not directly generate distortion but can amplify the existing distortion in the system, such as capacitors.

Therefore, standards to regulate the measurement of harmonic distortion and imbalances in a microgrid are necessary. On one hand, IEC 61,000-2–2 [5] establishes the total harmonic distortion (THD) as the index for measuring harmonic distortion in both voltage and current, specifying the maximum THD values at any point in the grid and also setting the total imbalance level. Commercial PQ analysers enable the measurement of the THD index at the point of common connection (PCC) [6–8]. On the other hand, IEEE Standard 1459 [9] offers methods for measuring electric power in unbalanced conditions. However, these standards and the indices derived from them are insufficient for identifying the sources of distortion or imbalance sources in a microgrid.

To overcome this drawback, several procedures and algorithms have been published over the last decades to identify sources of distortion [10–14]. Current best practices have evolved beyond normative approaches, incorporating data-driven and advanced signal processing techniques. For instance, state-of-the-art methods now employ sparse signal recovery and compressive sensing to localize harmonic sources with limited measurement points, significantly enhancing identification accuracy in complex grid topologies [15]. Similarly, regarding

* Corresponding author.
E-mail address: jesus.clavijo@die.uhu.es (J. Clavijo-Camacho).

https://doi.org/10.1016/j.epsr.2026.112954
Received 13 October 2025; Received in revised form 2 March 2026; Accepted 8 March 2026
Available online 11 March 2026

Nomenclature

Abbr.	Meaning	Abbr.	Meaning
DSI	Distortion Source Identifier	HC	Host Computer
ISI	Imbalance Source Identifier	CB	Communication Board
HGI	Harmonic Global Index	VR	Voltage Regulator Load
NL	Non-Linear Index	DCVS	DC Voltage Source Load
LCI	Load Characterization Index	RLL	Balanced RL Load
UCR	Unbalance Current Ratio	URL	Unbalanced Resistive Load
THD	Total Harmonic Distortion	RCL	Balanced Capacitive Load
PCC	Point of Common Coupling	DGM	Distributed Generation Module
MD	Measurement Device	V_i	i th harmonic component of voltage
		I_i	i th harmonic component of current

imbalance [16–18], these methods require, at a minimum, the measurement of instantaneous voltage and current at all microgrid nodes [19].

Based on the above, an electrical measurement network that meets the measurement requirements necessary for PQ analysis, specifically for detecting harmonic and imbalance sources, is needed. The requirements imposed by the standards are as follows:

- According to the standards [3,20,21], voltage and current must be sampled at 128, 256 or 512 samples per cycle across 10 cycles, using high-speed analog-to-digital converters (ADCs) with a minimum sample rate of 12.8 kSPS and a signal-to-noise ratio (SNR) exceeding 86 dB.
- The measurements from different nodes must be simultaneous to assess and compare pseudo-stationary disturbances, which can vary over time. Harmonics and imbalance are considered pseudo-stationary disturbances.
- The measurement of voltage and current at the same node must be simultaneous to enable the calculation of the different power components.

Reviewing the technical literature on electrical measurement networks [22], introduces a system utilizing self-developed smart meters with advanced communication capabilities, but it lacks synchronous measurement across multiple points. In [23], the authors develop a system for high-frequency, synchronous electromagnetic interference (EMI) measurements across multiple locations; however, it falls short of providing synchronous measurements across multiple points in a microgrid and relies on expensive commercial oscilloscopes to measure voltages and currents. Furthermore [24], presents a measurement system designed for accurate and synchronized PQ monitoring in a real distribution grid.

However, the system has several limitations, including a lack of focus on microgrids, an absence of node-specific harmonic identification, and limited scalability and portability. Finally, while electrical measurement networks designed for industrial sites, as discussed in [25,26], are effective, they do not delve deeply into PQ issues or the detection and classification of both stationary and non-stationary PQDs [27].

Regarding the algorithms published in the technical literature to identify imbalance sources, there are only a few. In contrast, there are many more algorithms for identifying distortion sources in a microgrid, which can be classified according to different criteria. For example, one of those criteria is based on comparing the harmonics supplied by the source with those supplied by the load to determine whether the harmonic source is on the supply side or the load side. In this group is, for example, the harmonic global index (HGI), with significant relevance and applicable to single point systems [28,29], or to multi-point [19,30]. The significance of this index is underscored by recent reviews and research papers [11,31].

The current decomposition is the approach of a significant cluster of proposals [4,10,32]. The current can be divided into two components: the first one refers to the portion of the load that maintains system integrity free from distortion, while the distortion generated by part of that actual load is represented in the second component. In instances involving linear loads, only the first component is present, whereas both components exist in scenarios featuring non-linear loads. Moreover, it is imperative to examine multi-point indices including the toll-road model [33], in which various current or power measures are relied upon, or the Global Power Quality Index [19], amalgamating several single-point indices. These multi-point indices necessitate at least one single-point index for comparing the values corresponding to measurements taken at each node. Multi-point indices are the only group capable of identifying distortion sources in an electrical installation. However, they have additional requirements compared to the single point. For instance, the measurements at each node must be simultaneous. Therefore, an electrical measurement network is needed. In addition, the system should be based on low-cost devices, free-software, and open-hardware. In this way, all the nodes can be analysed, instead of considering pseudo-measurements originated by the lack of devices to take all those measurements.

1.1. The innovation provided by the present paper

This paper presents a complete system for collecting the necessary measurement aligned with standards to identify distortion and imbalance sources in a microgrid. The system is denominated NIDI (network for identifying distortion and imbalance). In addition, it has the following characteristics:

- It is a complete system comprised of a self-developed measurement device (MD), a communication network that includes hardware and software elements, and the software for the host computer (HC), which can be installed on numerous platforms.
- It has been designed and built using low-cost equipment, free software, and open hardware platforms.
- It is easily portable and can be connected to any type of microgrid, whether single or three-phase. It is not necessary to open circuits to install it because suitable current sensors are used.
- The analysis of the microgrid can be either punctual or continuous over time.
- It incorporates a robust communication network that maintains continuous connectivity among all MDs, facilitating measurements in noisy environments.
- To ensure accurate identification of distortion and imbalance sources, the influence of non-stationary disturbances must be eliminated. For this purpose, the MDs acquire 10 consecutive voltage and current cycles and select one that can be considered quasi-stationary.
- To identify this representative cycle, the RMS values, fundamental-frequency estimates, and phase angles of the 10 cycles are compared. A cycle is selected only if no significant amplitude,

frequency, or phase variations are detected. This mitigates the impact of voltage fluctuations and reduces spectral leakage effects arising from desynchronization between voltage and current. The voltage and current samples of the selected cycle are then used to compute the waveform spectra and apply the proposed identification algorithm.

- A new algorithm has been developed to calculate two new indices for identifying distortion and imbalance sources in electrical microgrids. These indices are named DSI (distortion source identifier) and ISI (imbalance source identifier), respectively. The DSI is a distributed index, and the ISI is concentrated. Both are based on the decomposition of the current at a node in the microgrid.

1.2. Paper organization

The paper is organized as follows: in Section 2, the materials and methods necessary to design, construct and test NIDI are presented. They are the published indices to identify distortion and imbalance sources and the experimental and simulation platforms to assess the effectiveness of NIDI. In Section 3, NIDI is presented since the MD to the algorithm developed to calculate the indices proposed for identifying distortion and imbalance sources. The results of using NIDI in the experimental and simulation platforms are presented in Section 4 and discussed in Section 5. Finally, in Section 6 some conclusions are depicted.

2. Materials and methods

This section is divided into two subsections. In the first, the most relevant indices in which the proposed in this paper are based on, are presented. In the second, the platforms designed and built to test the proposed indices are described.

2.1. Procedures to identify distortion and imbalance sources published in the technical literature

A complete study of the indices published in the technical literature to identify both distortion and imbalance sources in electrical installations is presented in [34]. This paper concludes that there is only one tandem of indices useful for this objective: LCI/UCR (load characterization index / unbalance current ratio). These indices where presented in [10,16,17] by the authors of the present paper.

LCI/UCR are based on the decomposition of the current at each node. They are concentrated indices that improve the results provided by other indices, such as HGI (harmonic global index) [28] and NL (non-linear index) [32], on which LCI is based. HGI and NL identify as distortion sources capacitive linear loads and LCI identify them as linear. All of them require only voltage and current measurements at the assessed node.

All these indices use the FFT (fast Fourier transform) and employ the harmonic components of each voltage and current, i.e., the voltage and current in frequency domain.

HGI decomposes the current into two complementary components, IS and IL, as shown in (1):

$$I_S + I_L = I \tag{1}$$

I_S involves the current harmonic components whose corresponding active power flows from source to load, and I_L the rest of current harmonic components. I is the current at the input of the node. Once the current is decomposed, the index HGI is calculated as shown in (2):

$$\mathrm{HGI} = \frac{\| I_L \|^2}{\| I_S \|^2} \tag{2}$$

where $\| \cdot \|$ denotes the Euclidean norm of the vector.

NL [32] also decomposes the current into two different components.

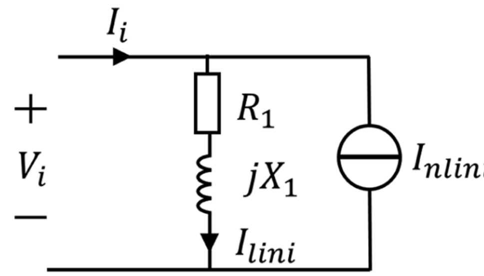

Fig. 1. Circuit representing the current decomposition corresponding to the NL index calculation and to the harmonic order *i*.

The first is named linear current, I_{lin}, and the second non-linear current I_{nlin} (which gives the index its name). To calculate the linear current, an impedance, Z, is calculated, whose first-order harmonic is the ratio of the fundamental component of voltage, V_1, and current, I_1, as shown in (3):

$$Z_1 = \frac{V_1}{I_1} \tag{3}$$

From Z_1, Z can be calculated for each other harmonic components, i, as shown in (4):

$$Z_i = R_1 + iX_1 \tag{4}$$

Once Z (vector composed of the different harmonic components of the impedance Z_i) is calculated, I_{lin} can be determined as the ratio of the voltage to impedance for each harmonic order, as shown in (5):

$$I_{\mathrm{lini}} = \frac{V_{\mathrm{i}}}{Z_{\mathrm{i}}} \tag{5}$$

where V_i is the i harmonic component of voltage. Thus, the electrical circuit corresponding to this current decomposition is shown in Fig. 1, considering the harmonic order *i*. The circuit structure remains the same for any harmonic order by modifying the value of *i*.

And so, $\boldsymbol{I_{nlin}}$ can also be calculated as shown in (6):

$$I_{\mathrm{nlin}} = I - I_{\mathrm{lin}} \tag{6}$$

Once the non-linear current is calculated, the NL index can be calculated as shown in (7):

$$\mathrm{NL} = \frac{\| I_{\mathrm{nlin}} \|}{\| I \|} \tag{7}$$

Neither of these two indices is able to identify linear loads composed of capacitors [35]. To overcome this limitation, LCI was introduced in [10,17]. LCI is calculated similarly to NL but with some differences. First, the calculation of Z, which will be referred to as $\boldsymbol{Z_{LCI}}$ for the case of calculating LCI, is the sum of three brunches. Second, the dual circuit is considered.

The circuit and the set of parameters corresponding to the option which gives value to LCI is used to calculated the index UCR as explained in [16].

The tandem LCI/UCR presents a higher performance than HGI or NL. However, their calculation is much more complex than the corresponding to the other.

2.2. Experimental and simulation setups for evaluating NIDI

To confirm that NIDI is a suitable electrical measurement network for identifying both distortion and imbalance sources, an experimental microgrid has been constructed comprising the following elements:

- An NHR® 9410 Regenerative Grid Simulator (referred to here as the grid emulator) that supplies a rated phase voltage of 230 V RMS at 50 Hz.

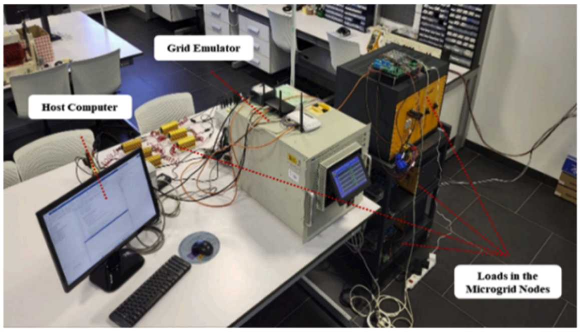

Fig. 2. Test bench configuration to validate the performance of NIDI.

Table 1
Specifications of the loads in the experimental microgrid nodes.

Node	Type of load	Values
Node 1. VR. Unbalanced distorting	Three single-phase regulators connected in star with inductive impedance on the right side. Distorting and unbalancing.	Phase 1: $R = 10$ Ω, $L = 0.1$ H Phase 1: $R = 12$ Ω, $L = 0.12$ H Phase 3: $R = 8$ Ω, $L = 0.08$ H
Node 2. DCVS. Distorting	Three-phase rectifier with a capacitive impedance on the DC side. Distorting.	$R = 100$ Ω $C = 0.2$ μF
Node 3. RLL	Three balanced inductive loads (a resistor in series to an inductance) connected in star	$R = 6.67$ Ω $L = 21.22$ mH
Node 4. URL. Unbalanced	Three unbalanced resistors connected in star. Unbalancing.	Phase 1: $R = 80$ Ω Phase 2: $R = 64$ Ω Phase 3:$R =$ 160 Ω

- Four microgrid nodes representing linear, nonlinear, balanced and unbalanced three-phase loads.

The photograph of the experimental platform is presented in Fig. 2. Details about the loads at each microgrid node are provided in Table 1, which shows the type of load and its expected contribution to distortion and imbalance, or its absence. Each load represents a microgrid node, and all four loads are connected to the grid emulator.

To extend the scope of the study, which is limited in the experimental tests to the values of the loads presented in Table 1, a simulation platform has been designed. It includes the same loads listed in Table 1, with two else: a capacitive balanced linear load (RCL) composed of three impedances of a 266.7 Ω resistor in parallel to a 0.119 mF capacitor connected in star, and a power generation module emulating a photovoltaic system (DGM). The parameter values shown in Table 1 were selected to reproduce representative distortion and imbalance conditions that commonly occur in real microgrids. In particular, the impedances of the voltage regulator (VR) were configured to generate both harmonic distortion and phase unbalance, conditions frequently encountered in microgrids supplying inductive, power-electronic, and voltage-regulated loads. The DCVS parameters were chosen to emulate the typical non-linear current profiles produced by diode-based rectification stages with capacitive filtering, which constitute one of the main sources of harmonic distortion in low-voltage microgrids. The RLL and URL loads were defined to provide, respectively, a balanced linear reference condition and a purely resistive unbalanced condition, allowing the correct validation of both distortion- and imbalance-related indices

In this way, the performance of the indices can be tested for this problematic type of load/generation module.

The three-phase waveforms for the simulated loads are shown in Fig. 3. The voltage is the same for all loads, as they are connected to the same PCC, and it is both balanced and sinusoidal. The current at the input of the voltage regulator (VR) is unbalanced and non-linear (Fig. 3a); at the input of the direct current voltage side (DCVS), current is balanced and non-linear (Fig. 3b); at the input of the RL load (RLL), it is balanced and linear (Fig. 3c); for the unbalanced R load (URL), it is unbalanced and linear (Fig. 3d); for the RC load (RCL), it is balanced and non-linear (Fig. 3e); and for the distributed generation module (DGM), it is balanced and almost sinusoidal. Each current aligns

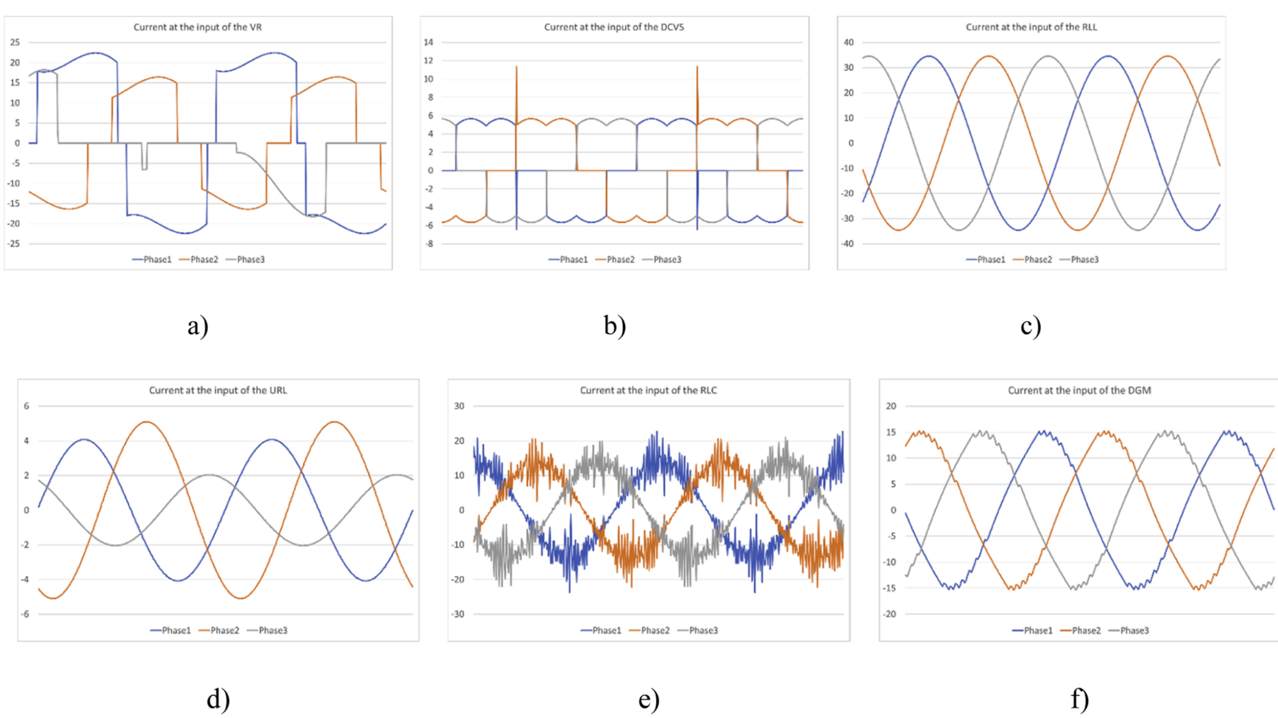

Fig. 3. Three-phase waveforms of currents at the input of: a) node 1, b) node 2, c) node 3, d) node 4, e) node 5 and f) node 6.

with the specific characteristics of its corresponding load except RCL, which is not non-linear but amplifies the existing distortion at its input.

3. Developed system for identifying distortion and imbalance sources

NIDI comprises as many MDs as there are nodes in the microgrid, as detailed in the paper [36], published by the authors of the present paper. Each MD is connected to an HC via a communication board (CB). Each element is detailed below.

In the proposed MD, the voltage sensor ZMPT101B and current sensor SCT-013 are used. The ZMPT101B is a compact voltage measurement module based on a high-isolation voltage transformer, providing stable measurements, excellent electrical isolation, and low losses compared to other low-cost voltage sensing solutions [37]. On the other hand, the SCT-013 is a non-invasive current sensor based on the Hall effect. This makes it easy to connect to loads, as there is no need to open circuits. The most important features of the SCT-013 are its high linearity and fast response. In addition, it is very robust to external noise. The SCT-013 exhibits a typical bandwidth of approximately 0–3 kHz, which is suitable for capturing low- and mid-order harmonic components relevant to power-quality analysis.

Moreover, both sensors are low-cost and widely used for harmonic source detection [37,38], making them ideal for measurements in industrial applications due to their robust resistance to external noise. Therefore, both sensors provide adequate dynamic performance and frequency response for harmonic measurements in microgrid environments.

Analog signals from voltage and current sensors are conditioned via an analog front end (AFE), which is based on a filter composed of inductance and capacitor, and an operational amplifier. Once converted the analog signal to digital, it is processed by a dsPIC30F5011 low-cost digital signal controller (DSC). An SRAM memory in the DSC was used to temporarily save the collected voltage and current measurements. Communication from the DSC to other peripherals is enabled through the RS232 interface.

From the MD perspective, three tasks need to be enabled:

- Receiving the measurement configuration and data requests.
- Performing and temporarily saving the measurements.
- Transmitting the voltage and current measurements for further processing.

The selection of devices and their parameters for the MD prototype was guided by several key criteria: compatibility with established standards, the need for high measurement, accuracy and robustness in diverse industrial environments. In addition, the use of low-cost, open-source hardware platforms such as the DSC enhances scalability, cost-effectiveness and integration into various microgrid configurations [36]. The RS232 communication protocol was selected for its robustness in handling noise, making it particularly suitable for electrically noisy environments, such as industrial settings.

The MD is programmed to transmit and receive data to and from the CB which acts as a bridge between the MD and the HC, which is responsible for initiating requests and processing data collected from the NIDI nodes. As CB, a Raspberry Pi® 4 Model B is used. The communication between the CB and the MD is via RS232 interface. Communication between the CB and the HC is wireless. Both are connected to the Internet using an RJ45 cable and share the same local area network (LAN). Using a LAN has several benefits, including data security, reduced interference and noise affecting the data transmission, easy and fast communication, and the ability to connect devices to the same network without requiring a physical connection among them. The WebSocket communication between each CB and the HC operates entirely within a dedicated isolated LAN, without external routing, ensuring that data exchange is confined to authenticated devices participating in the measurement system.

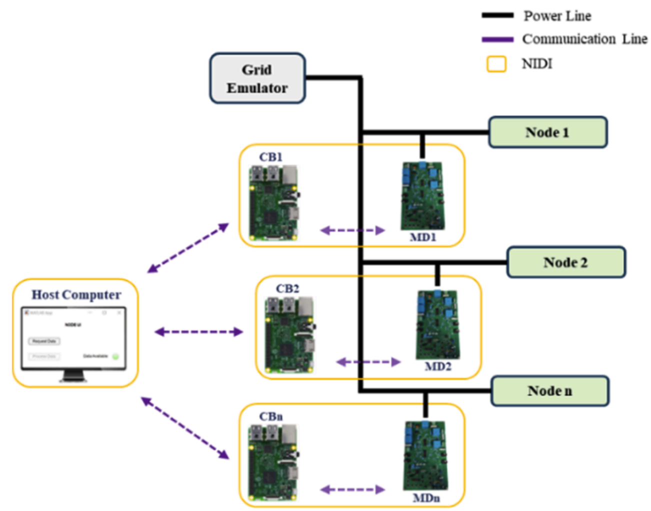

Fig. 4. NIDI connected to an experimental microgrid.

As a requirement, the voltage and current measurement from the MDs must satisfy two levels of simultaneity.

At the node level, each MD must acquire voltage and current measurements across all phases involved, i.e., three phases plus neutral for both voltage and current, at the same instant. This intra-node simultaneity is essential to ensure accurate unbalance and distortion analysis at each measurement point within the microgrid. Intra-node simultaneity is achieved by exploiting the simultaneous sampling mode of the dsPIC30F5011 ADC module, which features four Sample-and-Hold amplifiers that are triggered concurrently, allowing all voltage and current measurements at each node to be captured at the same time instant.

At the system level, all MDs deployed across the microgrid must acquire their measurements simultaneously. This inter-node simultaneity is critical for the correct assignation of responsibilities for unbalance and harmonic distortion to each load connected in the microgrid. For inter-node simultaneity, an NTP (network time protocol) server was installed on each CB. The NTP server disciplines the system clock of each CB by continuously adjusting it against a reference time source. The HC is configured as an NTP client, periodically querying each CB's NTP server to align its own clock, ensuring that all nodes in the measurement system share a common time reference. For parallel data processing, the HC implements parallel computing using MATLAB's Parallel Computing Toolbox. This allows the HC to handle the simultaneous reception and processing of data streams arriving from multiple CBs concurrently, by distributing computational tasks across multiple workers.

In a scenario with multiple loads, the connection of NIDI is depicted in Fig. 4. Once the voltage and current measurements are transferred to the HC, they are processed using the algorithm described in Section 3.1.

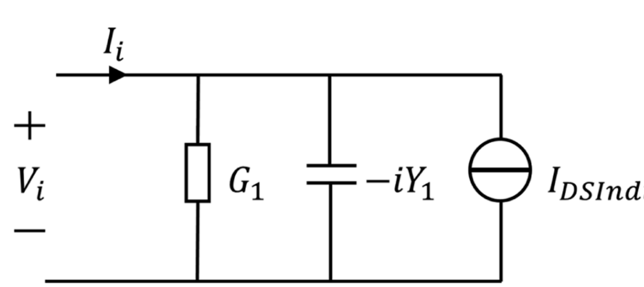

Fig. 5. Capacitive circuit considered to calculate DSI.

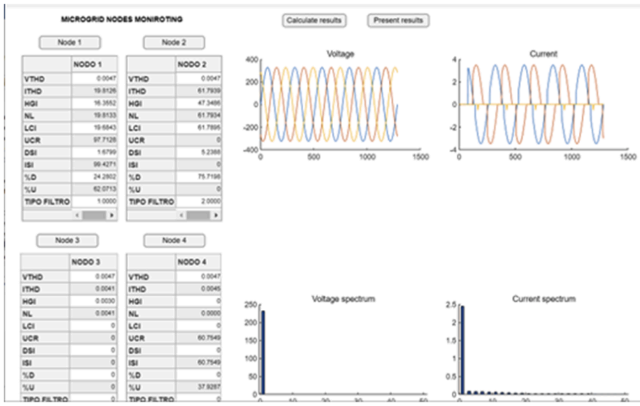

a)

	Node 1. VR	Node 2. DCVS	Node 3. RLL	Node 4. URL
V_{THD}	0	0	0	0
I_{THD}	19,81	61,79	0	0
HGI	16,36	47,35	0	0
NL	19,81	61,79	0	0
DSI	1,68	5,24	0	0
ISI	99,43	0	0	60,76
LCI	19,68	61,79	0	0
UCR	97,71	0	0	60,76

b)

Fig. 6. Results provided by NIDI when applied to the microgrid shown in Fig. 2: a) From monitoring application b) Distortion and imbalance indices computed for each node.

3.1. Proposed algorithm to identify sources of distortion and imbalance

The pair of indices proposed in this paper is as straightforward as HGI or NL and yields results as good as those of LCI/UCR, while identifying both distortion and imbalance sources. In fact, the calculation method is similar to that of NL but depends on the nature of the load at the input of the considered node. For inductive loads, the circuit depicted in Fig.1 is used; for capacitive loads, the circuit in Fig. 5 is used. Unlike LCI/UCR, only one set of parameters is considered. Thus, the fundamental component of the impedance is calculated as shown in (8):

$$Z_1 = \frac{V_1}{I_1} \text{ if } \sin(\varphi_{V_1} - \varphi_{I_1}) > 0$$

$$G_1 + jY_1 = \frac{I_1}{V_1} \text{ if } \sin(\varphi_{V_1} - \varphi_{I_1}) < 0 \quad (8)$$

where Z_1=R_1+jX_1 represents the impedance of the circuit depicted in Fig. 1, corresponding to the ratio of the voltage to the current's fundamental components at the input of the node. G_1 and Y_1 are the elements of the circuit shown in Fig. 5, corresponding to the ratio of the current to the voltage's fundamental components. G_1 is the real part of the ratio, and Y_1 is the imaginary part. φ_{V1} is the phase of the voltage's fundamental component, and φ_{I1} corresponds to the phase of the current's fundamental component.

The impedances of linear branches for a given harmonic order can be calculated by retaining the real part and multiplying the imaginary by the harmonic order. Consequently, the harmonic component of the current can be calculated as shown in (9):

$$\mathrm{I}_{\mathrm{lin}i} = \frac{V_i}{R_1 + j(iX_1)} \text{ if } \sin(\varphi_{V_1} - \varphi_{I_1}) > 0$$

$$\mathrm{I}_{\mathrm{lin}i} = V_i G_1 + jV_i(iY_1) \text{ if } \sin(\varphi_{V_1} - \varphi_{I_1}) < 0 \quad (9)$$

where I_{lini} represents the order i harmonic of the linear component of the current at the input of the node. The non-linear component of the current I_{DSInli} and the distortion ratio (DRatio) for each node are calculated as presented in (6) and (7), respectively. These equations are reformulated with the new designations as shown in (10) and (11):

$$\boldsymbol{I}_{\mathrm{DSInl}} = \boldsymbol{I} - \boldsymbol{I}_{\mathrm{lin}} \quad (10)$$

$$DRatio = \frac{\| \boldsymbol{I}_{DSInl} \|}{\| \boldsymbol{I} \|} \quad (11)$$

This new index considers the inductive or capacitive character of the fundamental impedance component at each node, unlike the NL algorithm. Once the values of DRatio for all nodes and the head are known, the value of the distortion source identifier (DSI) is calculated as the ratio of DRatio for each node to that of the head, as presented in (12).

$$DSI_n = \frac{DRatio_n}{DRatio_{head}} \quad (12)$$

where n represents each node, and 'head' refers to the values corresponding to the head of the microgrid.

Once the circuit is defined and the index DSI, is calculated, the previously established circuit is used to calculate the ISI index as follows.

Up to this point, all the electrical magnitudes considered are three-phase. To calculate ISI, the three-phase linear current, derived from the circuit represented in either Fig. 1 or Fig. 5 according to (9), is assessed. The phase with minimum fundamental component is identified (I_{1ISI}). From this, an equivalent balanced impedance is calculated as shown in (13):

$$Z_{1\mathrm{ISI}} = \frac{V_1}{I_{1ISI}} \quad (13)$$

From this impedance, the balanced I_{b1} and unbalanced I_{u1} fundamental currents are calculated for each phase m, as shown in (14) and (15):

$$I_{\mathrm{b1m}} = \frac{V_{1\mathrm{m}}}{Z_{1\mathrm{ISI}}} \quad (14)$$

$$I_{\mathrm{u1m}} = I_{1\mathrm{m}} - I_{\mathrm{b1m}} \quad (15)$$

Finally, ISI is calculated as shown in (16):

$$\mathrm{ISI} = \frac{\| I_{\mathrm{u1}} \|}{\| I_{\mathrm{lDSI1}} \|} \quad (16)$$

4. Results provided by NIDI

In this section, the results obtained by applying NIDI to both experimental and simulation platforms, as described in Section 2.2, are presented.

4.1. Results from applying NIDI to the experimental platform

The results obtained by applying NIDI to the experimental platform, as described in Section 2.2, are shown in Fig. 6. Fig. 6a) displays the output of the developed monitoring application, including the measured

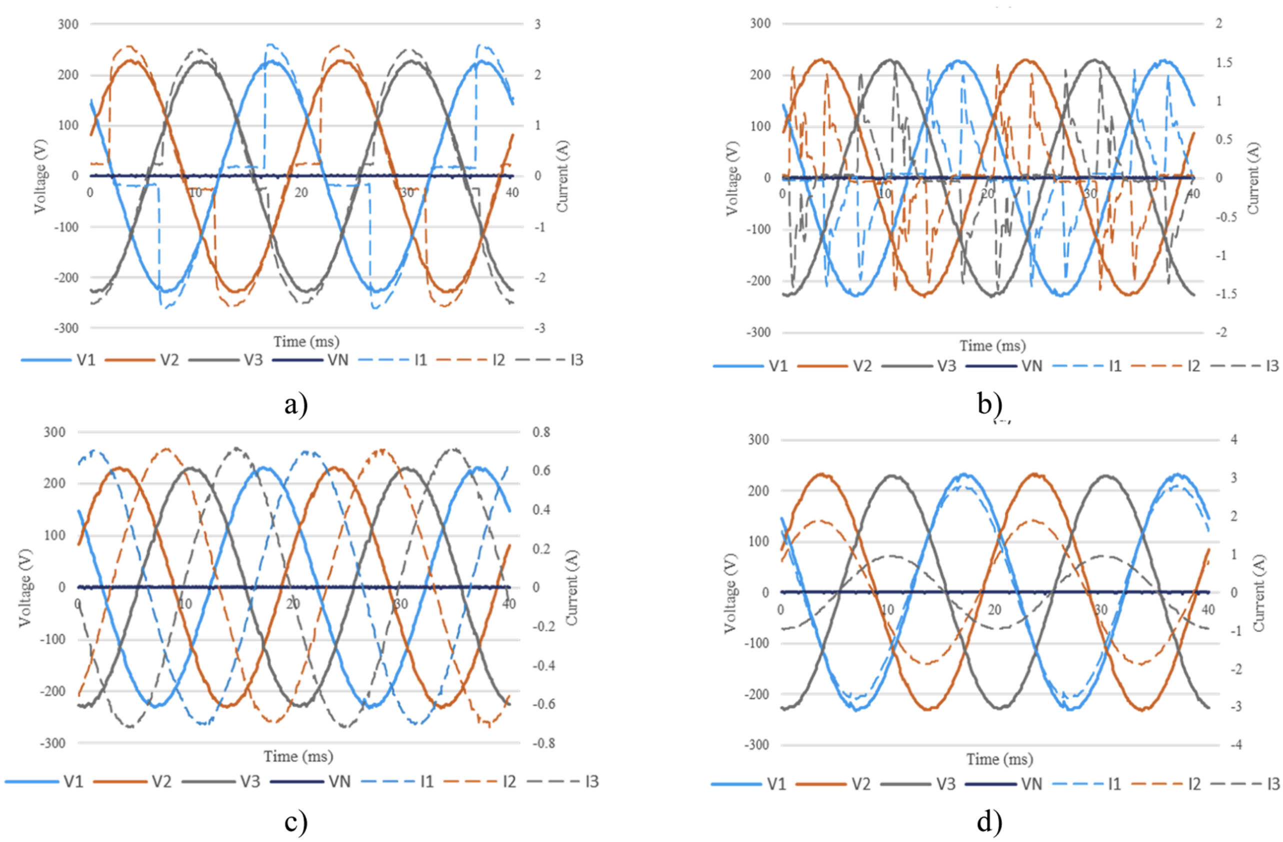

Fig. 7. Current waveforms, a) node 1, b) node 2, (c) node 3, d) node 4.

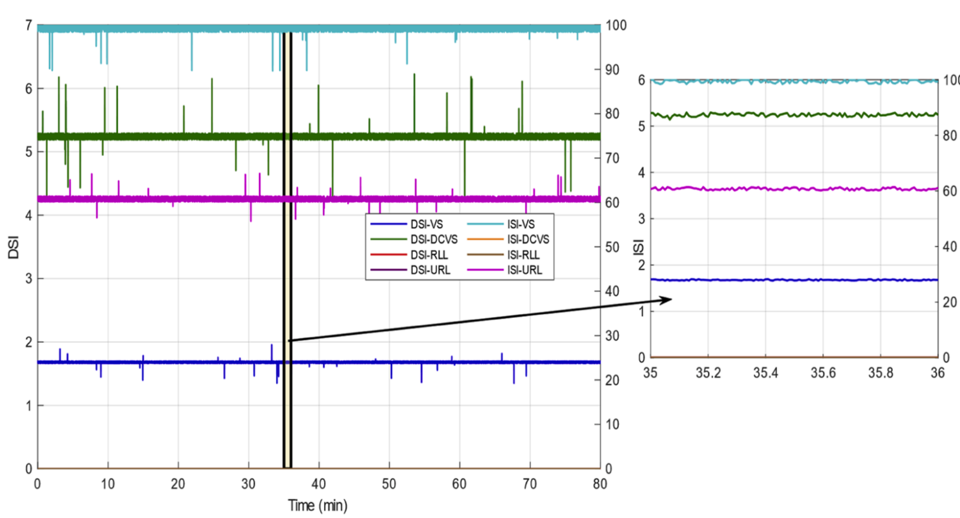

Fig. 8. Results of the prototype continuously monitoring the experimental microgrid.

voltage and current waveforms and their corresponding spectra. Fig. 6 b) presents the numerical values of the distortion and imbalance indices computed for each node, facilitating a clearer comparison among them. The graphs are the three-phase waveforms and one phase spectra of voltage and current corresponding to each node. The current waveforms are recrewed in Fig. 7. It is observed that nodes 1 and 2 introduce distortion into the grid, while the remaining nodes represent linear loads.

According to the tables in Fig. 5, DSI values are above zero for nodes 1 and 2, while ISI values are elevated for nodes 1 and 4, akin to the LCI/UCR indices. Similarly, HGI and NL indices also show values higher than zero for nodes 1 and 2.

The loads were then connected directly to the laboratory's electrical network, and the electrical values at the various nodes were monitored. The results provided by the experimental prototype are shown in Fig. 8, where it can be seen that the index values for the different types of loads remain constant over time.

This is because the laboratory network is robust and the loads are stationary, but this method demonstrates the prototype's ability to continuously monitor a microgrid.

Table 2
Value of indices provided by the simulation platform in the initial case.

	VR	DCVS	RLL	URL	RCL	DGM
HGI	9.87	58.95	0	0	7.71	3348.81
NL	19.81	61.90	0	0	7.92	4.12
DSI	2.02	6.31	0	0	0	0
ISI	99.43	0	0	60.75	0	0
LCI	19.64	61.89	0	0	0	4.12
UCR	28.50	0	0	7.193	0	0

4.2. Results from applying NIDI to the simulation platform

The results from applying NIDI to the simulation platform indicate the system's effectiveness, as detailed in Tables 2 and 3. In the initial case, as seen in Table 2, the indices identify VR and DCVS as distortion sources, with values higher than zero for HGI, NL, LCI, and DSI, while UCR and ISI detect imbalance in VR and URL. Also, HGI and NL take values higher than zero for RCL and HGI, NL and LCI for DGM.

Remember that the initial case is the same as the experimental platform, except that the simulation includes RCL and DGM.

Further testing is possible using the simulation platform with modified load parameters. In this way additional insight is provided. Case 1 involved changing the RCL resistor values from 10.7 to 533 Ω (Table 3 first case), and Case 2 involved a widespread of values for the DCVS resistance (Table 3 second case), from 4 to 600 Ω. In this way, many more cases can be analysed, and the NIDI performance is clearly verified.

Table 3 presents the mean values provided by all the indices for each node in the simulation platform in the first row and the standard deviation in the second row of each node. As can be seen, HGI, NL, LCI and DSI provide values higher than 0 for VR and DCVS, and so they are identified as distortion sources by those indices. It is striking that the DSI value is much lower than that of the other indices. It is because the DSI is the only distributed index (calculated respect to the head of the microgrid). Those indices identify as linear loads RLL and URL because the mean value provided by them is null in all the cases. With respect to RCL, which is a linear capacitive load, the indices present different results as follows:

HGI and NL identify this load as distortion sources versus LCI and DSI which considered the load as linear.

Regarding indices which identify imbalance sources, UCR and ISI, they identify as imbalance sources VR and URL, in which they provide values higher than zero. The data provided by these indices corresponding to the other nodes are null, as can be seen in Table 3.

To complete the test of NIDI and considering that in a microgrid the PCC voltage is not always sinusoidal and balanced (above all if they are connected to weak distribution systems), the results of using NIDI with the simulation system in the initial case are presented with increasing voltage distortion and increasing voltage imbalance in Table 4 first and second cases, respectively. None of the indices identify the RLL as distortion or imbalance source in none of the cases studied. HGI, NL, LCI and DSI identify VR and DCVS as distortion source and UCR and ISI identify VR and URL as imbalance source. Also, for the RCL the results provided by the different indices are not correct. In fact, HGI and NL identify RCL as distortion source for all the cases studied, and also LCI for some of those cases. And it is identified as imbalanced source by UCR and ISI in some cases, too. Finaly, with respect to DGM, it is considered distortion source by all the indices except DSI in any of the studied cases. In addition, DGM is considered as an imbalance source by UCR with increasing distorted and unbalanced voltage, and by LSI with the highest level of unbalanced voltage. Nevertheless, the values provided by LSI and UCR for DGM are much lower than those provided for URL.

It is also worth noting that harmonic distortion, typically quantified through THD, is directly associated with additional energy losses in

Table 3
Results of applying nidi to the simulation platform with a continuous change of some parameters.

		RCL R variable						**DCVS R variable**					
		HGI	NL	DSI	ISI	LCI	UCR	HGI	NL	DSI	ISI	LCI	UCR
VR	M	28	32	2	60	31	2	28	32	2	60	31	2
	D	0	0	0	0	0	0	1	0	0	0	0	0
DCVS	M	13	30	2	0	30	5	12	29	2	0	28	3
	D	0	0	0	0	0	0	1	1	0	1	6	2
RLL	M	0	0	0	0	0	0	0	0	0	0	0	0
	D	0	0	0	0	0	0	0	0	0	0	0	0
URL	M	0	0	0	54	0	31	0	0	0	54	0	31
	D	0	0	0	0	0	0	0	0	0	0	0	0
RCL	M	8	9	0	0	0	1	8	9	0	0	0	1
	D	1	1	0	0	0	0	0	0	0	0	0	0
DGM	M	3368	4	0	0	4	0	3439	4	0	0	4	0
	D	41	0	0	0	0	0	97	0	0	0	0	0

Table 4
Evolution of the values of studied indices with increasing voltage distortion in PCC (column 1) and with increasing voltage imbalance (column 2).

		Increasing voltage distortion						**Increasing voltage imbalance**					
		HGI	NL	DSI	ISI	LCI	UCR	HGI	NL	DSI	ISI	LCI	UCR
VR	M	25	31	2	60	31	10	26	32	2	60	31	2
	D	4	0	0	0	0	16	3	0	0	0	0	0
DCVS	M	27	31	2	0	31	33	12	29	2	1	29	6
	D	2	1	0	0	1	23	1	0	0	1	0	3
RLL	M	0	0	0	0	0	0	0	0	0	0	0	0
	D	0	0	0	0	0	0	0	0	0	0	0	0
URL	M	0	0	0	54	0	31	0	0	0	54	0	32
	D	0	0	0	0	0	0	0	0	0	0	0	0
RCL	M	16	19	0	0	0	0	9	10	0	0	0	0
	D	4	7	0	0	0	0	1	1	0	0	0	0
DGM	M	3546	5	0	0	5	1	5073	3	0	3	3	1
	D	240	1	0	0	1	1	780	0	0	2	0	1

Table 5
Results provided by the prototype with extreme distorted voltage imposed in simulation.

		Increasing voltage distortion					
		VR	DCVS	RLL	URL	RCL	DGM
Clipped	DSI	1.51	1.38	0	0	0	1.11
	ISI	99.9	1.44	0	53.75	0	2.14
Clipped+Square	DSI	5.03	3.02	0	0	0	2.18
	ISI	99.9	0	0	53.75	0	0

conductors, transformers, and power-electronic converters. Although NIDI focuses on locating the sources of distortion rather than computing energy-loss metrics, identifying the responsible nodes enables subsequent mitigation actions that reduce both THD levels and the corresponding losses.

To conclude this study, and to evaluate the robustness of the proposed indices under extremely adverse grid conditions, Table 5 shows the results provided by the prototype when a clipped voltage with a saturation value of 150 V is imposed in simulation, along with a simultaneous disturbance of the same clipper and a square wave. This low-voltage, highly degraded scenario represents a worst-case condition for power quality analysis, emulating severe real-world anomalies such as deep magnetic core saturation in distribution transformers or heavy non-linear overloading in weak microgrids. It can be observed that in the first case, the system identifies the sources of distortion and imbalance even if the disturbance is permanent (which is unusual). In the second case, the prototype provides adequate results if the disturbance lasts <120 ms (6 cycles). If the disturbance lasts longer, the system outputs a zero value for all loads. The value is restored once the disturbance ends. Note that this second imposed disturbance corresponds to a voltage THD value of over 40 %. Fig. 9

5. Discussion

NIDI is a platform (experimental prototype) which comprises all the hardware and software needed to identify distortion and imbalance sources in a microgrid. The algorithm proposed for that by NIDI is the pair DSI/ISI. The results of the other indices are presented to compare the results provided by NIDI and those obtained by applicating other known indices. Thus, the results obtained from the application of NIDI to both the experimental and simulation platforms show its ability to identify distortion and imbalance sources in microgrids.

Regarding the experimental platform, which comprises usual loads in a microgrids, NIDI provide excellent results. The simulation platform allows an expanded analysis by including a wider range of load types and varying parameters.

The results obtained also corroborate the good perform of NIDI to identify distortion and imbalance source. As an exception, only in a few cases from all the presented in Section 4, ISI identifies the DCVS and the DGM as imbalance source, erroneously, although with values much less than those corresponding to true imbalance sources as URL. In the rest of cases studied, the results of NIDI to identify imbalance sources are excellent, as well as to identify distortion sources. Even with power generating modules among the assessed nodes.

The pair LCI/UCR is the only from the other indices analysed which presents results comparable to the pair DSI/ISI, used by NIDI. Nevertheless, the algorithm used to calculate LCI/UCR is much more complicated than the used to calculate DIS/ISI. This fact tips the balance again in favour of the proposed pair, reinforcing its superiority.

These good results have also been corroborated in microgrids with distorted or unbalanced voltage in the PCC, which usually correspond to microgrids connected to weak distribution power systems, and in the presence of transitory disturbances.

Overall, the results from both experimental and simulation platforms illustrate the performance of NIDI in detecting and classifying distortion and imbalance sources in microgrids, and the system's ability to accurately identify disturbances under various conditions was demonstrated.

6. Conclusions

The increasing importance of PQ makes necessary monitor the microgrids from the point of view of the supplier as well as from the corresponding to consumer. Thus, an electrical measurement network which can be scalable, portable and easy installed in any type of microgrid is necessary. It also would meet the requirements of the standard procedures for measuring electrical parameters and perform power quality analysis. This paper presents an experimental prototype that measures voltage and current at each node of a microgrid with the necessary characteristics to identify distortion and/or imbalance sources in microgrids.

The system, called NIDI, is composed of a HC and as many MDs as nodes there must be assessed in the microgrid. All those MDs are wireless connected to the HC through WebSocket implemented in CBs which acts as bridges. The structure of NIDI makes it a complete and versatile system, easily portable, and connectable, and based on low-cost elements. A new algorithm which improves the technical literature has been developed to identify both distortion and imbalance sources.

In addition, the experimental results obtained of using NIDI in the microgrid designed and built ad hoc, verify its good performance to identify the harmonic sources in a microgrid. These tests have been improved with a complete simulation study, including a power generation module. Results prove the good performance of NIDI to identify both distortion and imbalance sources in any kind of microgrid. Since harmonic distortion (THD) is inherently associated with additional

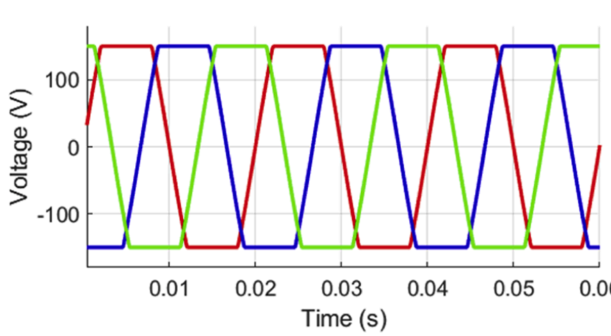

a)

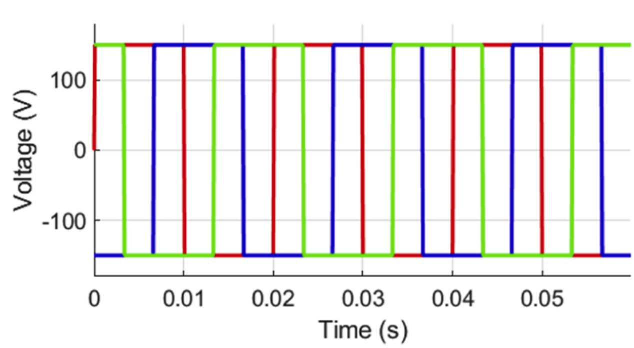

b)

Fig. 9. Applied voltage waveforms: a) Clipped sine, b) Combined clipped and square wave.

energy losses in conductors and electromagnetic devices, the capability of NIDI to determine the origin of such distortion provides valuable information for subsequent loss-mitigation actions in practical microgrid environments.

Future work will extend the validation of NIDI by deploying the system in an operational microgrid, enabling its assessment under real-world operating conditions and further consolidating its applicability in practical environments.

CRediT authorship contribution statement

Reyes Sánchez-Herrera: Writing – original draft, Supervision, Investigation, Funding acquisition, Data curation, Conceptualization. **Gabriel Gómez-Ruiz:** Writing – review & editing, Methodology, Investigation, Conceptualization. **Jesús Clavijo-Camacho:** Writing – review & editing, Software, Investigation, Formal analysis. **José A. Hernández-Torres:** Validation, Resources, Investigation, Formal analysis. **Álvaro Cruz-Álamo:** Writing – review & editing, Validation, Methodology, Investigation. **Nicolás Magro:** Writing – review & editing, Software, Formal analysis, Conceptualization. **Jesús R. Vázquez:** Writing – review & editing, Project administration, Methodology, Investigation, Data curation.

Declaration of competing interest

The authors declare that they have no known competing financial interests or personal relationships that could have appeared to influence the work reported in this paper.

Acknowledgements

This work is framed in the project "Development of a system based on Industrial IoT for the analysis of electrical power in power systems", grant number UHU-202023, funded by the European Commission (EU), the University of Huelva (Q7150008F) and the Andalusia Government (S4111001F). In addition, Gabriel Gomez-Ruiz is enjoying an FPU grant funded by the Spanish Ministry of Universities for training of university teaching staff in his PhD period. The author Jesus Clavijo-Camacho is participating in a INVESTIGO research fellowship funded by the European Union – NextGenerationEU. Funding for open access charge: Universidad de Huelva / CBUA.

Data availability

Data will be made available on request.

References

[1] S. Bhattacharyya, S. Cobben, S. Bhattacharyya, S. Cobben, Consequences of Poor Power Quality – An Overview, IntechOpen, 2011, https://doi.org/10.5772/13787.

[2] R. Igual, C. Medrano, Research challenges in real-time classification of power quality disturbances applicable to microgrids: a systematic review, Renew. Sustain. Energy Rev. 132 (2020) 110050, https://doi.org/10.1016/j.rser.2020.110050.

[3] EN 50160, Voltage characteristics of electricity supplied by public distribution network, (2022).

[4] D. Eltigani, S. Masri, Challenges of integrating renewable energy sources to smart grids: a review, Renew. Sustain. Energy Rev. 52 (2015) 770–780, https://doi.org/10.1016/j.rser.2015.07.140.

[5] IEC 61000-2-2, Compatibility levels for low-frequency conducted disturbances and signalling in public low-voltage power, supply systems (2002).

[6] 'Fluke Corporation: fluke electronics, calibration and networks'. Accessed: Jun. 21, 2023. [Online]. Available: https://www.fluke.com/.

[7] 'Home - circutor'. Accessed: Dec. 12, 2025. [Online]. Available: https://circutor.com/en/.

[8] 'PQube® 3 power analyzers \textbar powerside'. Accessed: Oct. 26, 2023. [Online]. Available: https://powerside.com/products/power-quality-measurement-solutions/pqube-3-power-analyzers/.

[9] 'IEEE standard for harmonic control in electric power systems', *IEEE Std 519-2022 (Revision of IEEE Std 519-2014)*, pp. 1–31, 2022, doi: 10.1109/IEEESTD.2022.9848440.

[10] R.S. Herrera, P. Salmerón, Harmonic disturbance identification in electrical systems with capacitor banks, Electr. Power Syst. Res. 82 (1) (2012) 18–26, https://doi.org/10.1016/j.epsr.2011.08.013.

[11] R. Sinvula, K.M. Abo-Al-Ez, M.T. Kahn, Harmonic source detection methods: a systematic literature review, IEEE Access 7 (2019) 74283–74299, https://doi.org/10.1109/ACCESS.2019.2921149.

[12] R.A.S. Fernandes, M. Oleskovicz, I.N. Da Silva, Harmonic source location and identification in radial distribution feeders: an approach based on particle swarm optimization algorithm, IEEE Trans. Ind. Inform. 18 (5) (2022) 3171–3179, https://doi.org/10.1109/TII.2021.3108681.

[13] G. Ye, Y. Xiang, V. Cuk, J.F.G. Cobben, Harmonic disturbance location by applying Bayesian inference, Electr. Power Syst. Res. 140 (2016) 886–894, https://doi.org/10.1016/j.epsr.2016.04.016.

[14] I.D. Melo, J.L.R. Pereira, A.M. Variz, P.A.N. Garcia, Harmonic state estimation for distribution networks using phasor measurement units, Electr. Power Syst. Res. 147 (2017) 133–144, https://doi.org/10.1016/j.epsr.2017.02.027.

[15] Z. Hu, Y. Han, A.S. Zalhaf, S. Zhou, E. Zhao, P. Yang, Harmonic sources modeling and characterization in modern power systems: a comprehensive overview, Electr. Power Syst. Res. 218 (2023) 109234, https://doi.org/10.1016/j.epsr.2023.109234.

[16] R.S. Herrera, J.R. Vázquez, Identification of unbalanced loads in electric power systems, Int. Trans. Electr. Energy Syst. 24 (9) (2014) 1232–1243, https://doi.org/10.1002/etep.1772.

[17] A.D. Martin, R.S. Herrera, J.R. Vazquez, P. Crolla, G.M. Burt, Unbalance and harmonic distortion assessment in an experimental distribution network, Electr. Power Syst. Res. 127 (2015) 271–279, https://doi.org/10.1016/j.epsr.2015.06.005.

[18] A. Pérez Vallés, P. Salmerón Revuelta, A new distributed measurement index for the identification of harmonic distortion and/or unbalance sources based on the IEEE Std. 1459 framework, Electr. Power Syst. Res. 172 (2019) 96–104, https://doi.org/10.1016/j.epsr.2019.03.007.

[19] L. Cristaldi, A. Ferrero, S. Salicone, A distributed system for electric power quality measurement, IEEE Trans. Instrum. Meas. 51 (4) (2002) 776–781, https://doi.org/10.1109/TIM.2002.803300.

[20] 'UNE-EN IEC 62053-21 - 2021-05-01 - DIN media'. Accessed: Dec. 12, 2025. [Online]. Available: https://www.dinmedia.de/en/standard/une-en-iec-62053-21/341081756.

[21] IEC 61850-3. Communication networks and systems for power utility automation - part 3: general requirements, 2013.

[22] Y.M. Mendi, H. Akinc, İ. Başalan, D. Atlı, Y. Civelek, Design and implementation of smart meters with hybride communication system architecture, in: 2019 IEEE PES Innovative Smart Grid Technologies Europe (ISGT-Europe), 2019, pp. 1–5, https://doi.org/10.1109/ISGTEurope.2019.8905774.

[23] A. Matthee, N. Moonen, F. Leferink, Synchronous multipoint low-frequency EMI measurement and applications, IEEE Lett. Electromagn. Compat. Pract. Appl. 4 (4) (2022) 120–124, https://doi.org/10.1109/LEMCPA.2022.3218320.

[24] Í.J. Batista, L.H.S.C. Barreto, Wireless web-based power quality monitoring system in a microgrid, in: 2018 Simposio Brasileiro de Sistemas Eletricos (SBSE), 2018, pp. 1–4, https://doi.org/10.1109/SBSE.2018.8395553.

[25] G.P. de Souza, W.do C. Boaventura, Time-alignment of electrical network measurements through time series of cycle RMS values, Int. J. Electr. Power Energy Syst. 144 (2023) 108518, https://doi.org/10.1016/j.ijepes.2022.108518.

[26] P. Castello, A. Murenu, P.A. Pegoraro, S. Sulis, Accurate measurement system for power quality monitoring in a real grid context, in: 2020 IEEE PES Innovative Smart Grid Technologies Europe (ISGT-Europe), 2020, pp. 1120–1125, https://doi.org/10.1109/ISGT-Europe47291.2020.9248855.

[27] Rahul, B. Choudhary, An advanced genetic algorithm with improved support vector machine for multi-class classification of real power quality events, Electr. Power Syst. Res. 191 (2021) 106879, https://doi.org/10.1016/j.epsr.2020.106879.

[28] C. Muscas, Assessment of electric power quality: indices for identifying disturbing loads, Eur. Trans. Electr. Power 8 (4) (1998) 287–292, https://doi.org/10.1002/etep.4450080411.

[29] T. Tanaka, H. Akagi, A new method of harmonic power detection based on the instantaneous active power in three-phase circuits, IEEE Trans. Power Deliv. 10 (4) (1995) 1737–1742, https://doi.org/10.1109/61.473386.

[30] E.J. Davis, A.E. Emanuel, D.J. Pileggi, Harmonic pollution metering: theoretical considerations, IEEE Trans. Power Deliv. 15 (1) (2000) 19–23, https://doi.org/10.1109/61.847223.

[31] F. Safargholi, K. Malekian, W. Schufft, On the dominant harmonic source identification— part I: review of methods, IEEE Trans. Power Deliv. 33 (3) (2018) 1268–1277, https://doi.org/10.1109/TPWRD.2017.2751663.

[32] A. Dell'Aquila, M. Marinelli, V.G. Monopoli, P. Zanchetta, New power-quality assessment criteria for supply systems under unbalanced and nonsinusoidal conditions, IEEE Trans. Power Deliv. 19 (3) (2004) 1284–1290, https://doi.org/10.1109/TPWRD.2004.829928.

[33] G.V. de Andrade, S.R. Naidu, M.G.G. Neri, E.G. da Costa, Estimation of the utility's and consumer's contribution to harmonic distortion, in: 2007 IEEE Instrumentation & Measurement Technology Conference IMTC 2007, 2007, pp. 1–5, https://doi.org/10.1109/IMTC.2007.379201.

[34] R. Sánchez-Herrera, J. Clavijo-Camacho, G. Gómez-Ruiz, J.R. Vázquez, Identification of both distortion and imbalance sources in electrical installations: a comparative assessment, Energies 17 (11) (2024) 11, https://doi.org/10.3390/en17112536. Art. no.

[35] N. Locci, C. Muscas, S. Sulis, On the measurement of power quality indexes for harmonic distortion in the presence of capacitors, in: 2005 IEEE

Instrumentationand Measurement Technology Conference Proceedings, 2005, pp. 1600–1605, https://doi.org/10.1109/IMTC.2005.1604437.
[36] G. Gómez-Ruiz, R. Sánchez-Herrera, A.D. Martin, J.M. Andújar, Optimum system for diagnosing power quality in electrical microgrids, Appl. Sci. 14 (17) (2024) 17, https://doi.org/10.3390/app14177666. Art. no.
[37] D.A. Elvira-Ortiz, D. Morinigo-Sotelo, A.L. Zorita-Lamadrid, R.A. Osornio-Rios, R. de J Romero-Troncoso, Fundamental frequency suppression for the detection of broken bar in induction motors at low slip and frequency, Appl. Sci. 10 (12) (2020) 4160, https://doi.org/10.3390/app10124160.
[38] M. Havrlík, M. Libra, V. Poulek, P. Kouřím, Analysis of output signal distortion of galvanic isolation circuits for monitoring the mains voltage waveform, Sens.(Basel Switz.) 22 (20) (2022) 7769, https://doi.org/10.3390/s22207769.